Fermilab Library
0 1160 0029261 2

DFF 194/11/93
November 1993

QCD AND JETS (THEORY) *

Stefano Catani
INFN, Sezione di Firenze, and
Dipartimento di Fisica dell'Università di Firenze,
Largo Fermi 2, I-50125, Firenze, Italy

DEC 20 1993

Contents 18

INTRODUCTION 1
HARD SCATTERING CROSS SECTIONS IN PERTURBATIVE QCD 1
Completely inclusive quantities: NNLO predictions and α_S determinations 1
NLO calculations for inclusive quantities 3
JET MEASURES IN e^+e^- ANNIHILATION 3
Shape variables 3
Jet cross sections 6
JET PHYSICS IN HADRON-HADRON COLLISIONS 7
Cone algorithms 8
Jet studies in NLO QCD 8
Alternative jet definitions 10
JETS IN ep COLLISIONS 11
Photoproduction 11
Final states in DIS 12
SUMMARY OF α_S DETERMINATIONS 13
OUTLOOK 15

*Plenary talk given at the International Europhysics Conference on High Energy Physics, Marseille, France, 22-28 July 1993.

QCD AND JETS (THEORY)

STEFANO CATANI
INFN, Sezione di Firenze, Largo E. Fermi 2,
I-50125 *Florence, Italy*

ABSTRACT

Recent theoretical developments in perturbative QCD and jet physics are reviewed. The comparison between the theoretical predictions and the experimental results from high-energy e^+e^-, ep and $p\bar{p}$ colliders is discussed.

Introduction

Recent theoretical and experimental progress in Quantum Chromodynamics (QCD), the quantum field theory of strong interactions, has been presented in 4 parallel sessions (with more than 40 talks) and in about 50 contributed papers at this Conference. Due to the limited amount of time and space, my contribution cannot be considered a comprehensive review of the subject. A list of general topics reviewed elsewhere includes structure functions (and small-x physics) [1], most of HERA physics [2] and spin physics in QCD [3]. In this talk I concentrate on the comparison between perturbative QCD and jet physics data from e^+e^-, $p\bar{p}$ and ep colliders. In particular, I shall discuss the impact of accurate theoretical predictions on the analysis of the experimental data and outline further theoretical developments necessary both for future QCD tests and for calculations of QCD background for new physics.

Hard scattering cross sections in perturbative QCD

The perturbative approach to hard-scattering cross sections is based on the parton model picture. Considering, for instance, the inclusive production of a single particle at high transverse momentum $p_\perp$ in the collisions of two hadrons (Fig. 1), and neglecting higher-twist corrections (contributions vanishing as an inverse power of $p_\perp$), one can write down the cross section as a convolution of non-perturbative structure (F) and fragmentation (D) functions and a hard cross section factor $\sigma_{\rm hard}$. The latter is dominated by momentum regions of the order of $p_\perp$ and hence, provided that $p_\perp \gg \Lambda$ (Λ being the QCD scale), it can be computed in QCD perturbation theory to the lowest order in the 'small' (due to asymptotic freedom) running coupling $\alpha_S(p_\perp) \sim (\beta_0 \ln p_\perp^2/\Lambda^2)^{-1}$.

This naive parton model approach predicts the order of magnitude of the cross section. The accuracy of the perturbative QCD expansion is instead controlled by the size of the higher-order corrections, as given by the

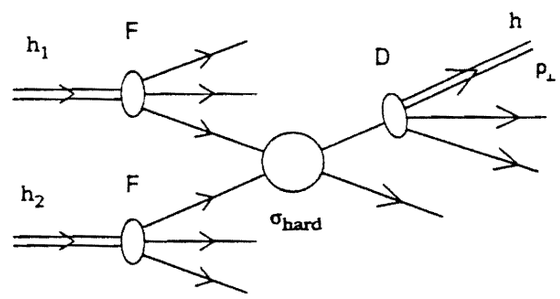

Fig. 1: The parton model picture of hard-scattering cross sections.

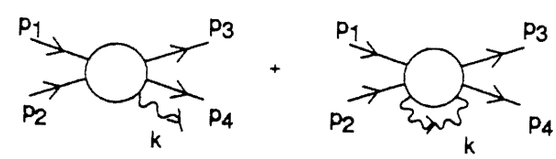

Fig. 2: Real and virtual NLO corrections for the hard-scattering process $p_1p_2 \to p_3p_4$.

emission of both real and virtual gluons (Fig. 2). In the computation of these corrections one has to deal with different kinds of singularities. The customary ultraviolet singularities, present in the virtual contributions, are removed by renormalization. By adding real and virtual terms, the infrared divergences cancel in inclusive cross sections, whilst the left over collinear singularities are factorized in the process independent structure and fragmentation functions $F(x, p_\perp^2)$ and $D(x, p_\perp^2)$, leading to predictable scaling violations.

Completely inclusive quantities: NNLO predictions and α_S determinations

Because of this complicated pattern of singularities, the simplest quantities which can be computed in QCD perturbation theory are the fully inclusive quantities, i.e. infrared and collinear safe observables depending on a single momentum scale. In this case only ultraviolet divergences appear and, at present, techniques

are available [4] to perform analytic calculations up to next-to-next-to-leading order (NNLO), i.e. to relative accuracy $\mathcal{O}(\alpha_S^3)$ with respect to the lowest-order approximation.

Quantities which have been evaluated to NNLO include the imaginary part $\mathrm{Im}\,\Pi^{(i)}(Q^2)$ of the correlation function of the vector ($i = V$) and axial ($i = A$) currents [5,6] (the relevant mass corrections $\mathcal{O}(m_q^2/Q^2)$ are also known [7]), the deep inelastic scattering (DIS) sum rules (namely the Gross-Llewellyn Smith sum rule and the polarized and unpolarized Bjorken sum rules) [8] and the $\mathcal{O}(\alpha_S^2)$ coefficient functions for the DIS [9] and Drell-Yan [10] processes (note however that in this case a consistent NNLO prediction requires the $\mathcal{O}(\alpha_S^3)$ anomalous dimensions, which are still unknown)*.

Fully inclusive quantities are expressed as a simple power series expansion in α_S and, therefore, they are particularly suitable for α_S determinations.

The imaginary part of the current-current correlation functions is directly proportional to the total hadronic cross section in e^+e^- annihilation. The experimental data in the centre-of-mass energy range from 20 to 65 GeV have been recently reanalysed by D. Haidt. Haidt's analysis [11] includes a *consistent* and *updated* treatment of electroweak radiative corrections as implemented in ZFITTER [12]. Using the perturbative QCD prediction for the vector part of the current correlation function (the axial part is negligible below the Z^0 resonance), Haidt obtains the following value for the strong coupling constant

$$\alpha_S(35\mathrm{GeV}) = 0.146 \pm 0.030 \ , \qquad (1)$$

where the error is dominated by the experimental uncertainty. The corresponding value evolved to the Z^0 mass, using the QCD running in NNLO [13], is $\alpha_S(M_Z) = 0.124 \pm 0.021$. Both the vector and axial parts instead contribute to the hadronic width $\Gamma_{\mathrm{had}}(M_Z)$ of the Z^0 vector boson. This quantity is therefore given by the non-factorized expression

$$\Gamma_{\mathrm{had}}(M_Z) = \Gamma^V_{\mathrm{ew}} R^V_{QCD} + \Gamma^A_{\mathrm{ew}} R^A_{QCD} \ , \qquad (2)$$

where $\Gamma^{V,A}_{\mathrm{ew}}$ include all the known electroweak contributions [14] and $R^{V,A}_{QCD} \sim \mathrm{Im}\,\Pi^{V,A}(M_Z^2)$ are the corresponding QCD corrections. Nonetheless, in the proper range of electroweak parameters, one can derive an approximate factorized expression. The factorized formula for the hadronic branching ratio of the Z^0 recently obtained by G. Passarino [15] is

$$R = \frac{\Gamma_{\mathrm{had}}(M_Z)}{\Gamma_{\mathrm{lep}}(M_Z)} \simeq R_0 \left[1 + 1.050^{+0.003}_{-0.002}\frac{\alpha_S}{\pi} + 1.136\left(\frac{\alpha_S}{\pi}\right)^2 - 12.805\left(\frac{\alpha_S}{\pi}\right)^3\right] ,$$
$$R_0 = 19.96^{+0.03}_{-0.04} \ , \qquad (3)$$

where the uncertainties on the $\mathcal{O}(\alpha_S)$ coefficient and R_0 refer to variations of the top and Higgs masses in the range $100\,\mathrm{GeV} < M_t < 200\,\mathrm{GeV}, 60\,\mathrm{GeV} < M_H < 1\,\mathrm{TeV}$. Including the data collected in the 1992 run, the new LEP average for R reported at this Conference [16] is $R = 20.781 \pm 0.049$. From this value and using eq. (3) one gets

$$\alpha_S(M_Z) = 0.120 \pm 0.007(\mathrm{exp.}) \pm 0.006(\mathrm{th.}) \ , \qquad (4)$$

where the central value corresponds to $M_t = 150\,\mathrm{GeV}$, $M_H = 300\,\mathrm{Gev}$ and the theoretical error is dominated by the uncertainty on the top mass. There is a slight discrepancy between the α_S value in eq. (4) and the corresponding official LEP average [16]

$$\alpha_S(M_Z) = 0.124 \pm 0.007(\mathrm{exp.}) \pm 0.006(\mathrm{th.}) \ . \qquad (5)$$

This discrepancy is enterely of 'theoretical' origin (and smaller than the present experimental accuracy): the value in eq. (5) is obtained again from the result in eq. (2) as numerically implemented in ZFITTER 4.6. I believe the origin of this discrepancy will be soon clarified.

An independent determination of α_S in NNLO can be obtained from the hadronic width of the τ lepton. Also this quantity is indeed related to the current correlation function via a simple momentum sum rule [17]. The corresponding hadronic branching ratio is given by

$$R_\tau = \frac{B(\tau \to \nu_\tau + \mathrm{had.})}{B(\tau \to \nu_\tau l \bar{\nu}_l)} = R^{(0)}[1 + \delta_{\mathrm{pert.}} + \delta_{\mathrm{non-pert.}}] \ , \qquad (6)$$

where $R^{(0)}$ is the parton model value and the perturbative QCD correction is

$$\delta_{\mathrm{pert.}} = \frac{\alpha_S}{\pi} + 5.2\left(\frac{\alpha_S}{\pi}\right)^2 + 26.4\left(\frac{\alpha_S}{\pi}\right)^3 \ . \qquad (7)$$

Since the τ mass M_τ is not very large, the non-perturbative higher-twist contribution in eq. (6) is potentially sizeable. An estimate [17], based on QCD sum rules, gives $\delta_{\mathrm{non-pert.}} = -0.02 \pm 0.01$. Using this value and the present world average for R_τ, one obtains [18]

$$\alpha_S(M_\tau) = 0.36 \pm 0.02(\mathrm{exp.}) \pm 0.04(\mathrm{th.}) \ , \qquad (8)$$

or, equivalently, $\alpha_S(M_Z) = 0.122 \pm 0.002(\mathrm{exp.}) \pm 0.004$ (th.). The very small theoretical uncertainty in eq. (8) heavyly relies on our understanding of the non-perturbative corrections. The good news that appeared during this year is that the estimated value of $\delta_{\mathrm{non-pert.}}$ has been found consistent with the measured hadronic mass spectrum of the τ lepton [19]. For this reason, I think

*As shown below, for all these observables the size of the computed coefficients in the α_S expansion (not α_S/π !) have been found to be of order unity.

we are now more confident about the determination (8) of α_S from τ decay.

The Gross-Llewellyn Smith sum rule can also be used to extract α_S. The NNLO theoretical prediction gives [8]

$$\int_0^1 dx[F_3^{\bar{\nu}p}(x,Q^2)+F_3^{\nu p}(x,Q^2)] = 6[1-\Delta_{\text{pert.}}-\Delta_{\text{h.t.}}] , \tag{9}$$

$$\Delta_{\text{pert.}} = \frac{\alpha_S}{\pi} + 3.58\left(\frac{\alpha_S}{\pi}\right)^2 + 19.0\left(\frac{\alpha_S}{\pi}\right)^3 , \quad (N_f = 3) . \tag{10}$$

Chyla and Kataev [20] used recent high precision data at $\langle Q^2 \rangle = 3\,\text{GeV}^2$ from the CCFR Collaboration [21] and the estimate $\Delta_{\text{h.t.}} = 0.032 \pm 0.016$ for the higher twist contribution from QCD sum rules to obtain

$$\alpha_S(1.73\text{GeV}) = 0.320 \pm 0.043(\text{exp.}) \pm 0.029(\text{th.}) \ . \tag{11}$$

Also in this case, due to the relatively low momentum region involved, the theoretical uncertainty is dominated by the higher-twist correction. A measurement of α_S from the Q^2-dependence of the Gross-Llewellyn Smith sum rule would be very interesting to confirm the result in eq. (11).

NLO calculations for inclusive quantities

QCD calculations beyond leading order for inclusive quantities are much more involved. Due to the complicated phase space for multi-parton configurations, analytic calculations are in practice impossible for most of the distributions. Moreover, infrared and collinear singularities, present in the intermediate steps, have to be first regularized by analytic continuation in a number of space-time dimensions $n = 4 + 2\epsilon$ different from four. This analytic continuation greatly complicates the Lorentz algebra and prevents a straightforward implementation of numerical integration techniques. Despite these difficulties, efficient computational algorithms have been set up [22], at least in next-to-leading order (NLO). Let me briefly sketch the basic points of the algorithms.

The NLO matrix element $|M_{\text{real}}(p_i,k)|^2$ for real emission (Fig. 2) is split in a regular and a singular part $|M_{\text{real}}|^2 = |M_{\text{reg.}}|^2 + |M_{\text{sing.}}|^2$ in the infrared and collinear limit. The regular part can be numerically integrated directly in four space-time dimensions, whilst only the singular part has to be evaluated analytically. The relevant simplification is that $|M_{\text{sing.}}|^2$ can be computed without any explicit NLO calculation in $n = 4 + 2\epsilon$ dimensions. This is because it can be obtained from the leading-order matrix element $|M(p_i)|^2$ by using universal infrared and collinear insertion factors. The corresponding factorization formulae [23] in the infrared and collinear limits respectively are

$$|M_{\text{sing.}}(p_i,k)|^2 = M^\dagger(p_i)[J(p_i;k)]^2 M(p_i) \ , \quad (k \to 0) \ , \tag{12}$$

$$|M_{\text{sing.}}(p_i,k)|^2 = |M(p_i)|^2 \frac{1}{p_i k} P_i(z;\epsilon) \ , \quad (k \to z p_i) \ , \tag{13}$$

where $J^\mu(p_i;k) = \sum_i T_i p_i^\mu / p_i k$ is the soft gluon current and $P_i(z;\epsilon)$ are the Altarelli-Parisi splitting functions.

Also the computation of the NLO matrix element for virtual emission can be at present greatly simplified. It has been realized that, in the infinite string tension limit, string theory provides an efficient bookkeeping of the Feynman diagrams of the corresponding massless field theory and new simplified techniques for evaluating one-loop amplitudes (although, so far, only in the case of external gluons) have been derived [24]. Using these techniques previous calculations of the one-loop 4-point amplitudes [25] have been checked and a new result, the one-loop 5-point gluon amplitude, has been obtained [26]. Although, it has been shown a posteriori that similar results can be derived directly from field theory [27], it is likely that string theory methods may continue to play a major role in inspiring simplified Feynman rules.

The extension to higher orders of the NLO techniques described so far is still an open problem and a challenge for theorists in this decade [28].

Having presented the general method to perform NLO calculations, in the following sections I shall discuss the comparison between these predictions and high-energy collider data.

Jet measures in e^+e^- annihilation

The most detailed QCD tests performed so far at e^+e^- colliders are based on studies of shape variables and jet cross sections.

Shape variables

The shape variables are global observables characterizing the structure of the hadronic final states. One of these variables is the thrust T, which is defined as

$$T = \underset{\mathbf{n}}{\text{Max}} \frac{\sum_i |\mathbf{p}_i \cdot \mathbf{n}|}{\sum_i |\mathbf{p}_i|} \ , \tag{14}$$

and thus maximizes the total longitudinal momentum (along the unit vector $\mathbf{n}$) of the final-state particles p_i in a given event. For a two-jet event we have $T = 1$, whilst a spherical event has $T = 1/2$. Many other shape variables can be defined [29], with the only constraint of being infrared and collinear safe observables. Once this

constraint is fulfilled, they can be computed in QCD perturbation theory and the non-perturbative contributions are nominally of the order Λ/Q (Q is the e^+e^- centre-of-mass energy). In the following I denote by y a generic shape variable whose two-jet limit corresponds to the region $y \to 0$ (for instance, $y = 1 - T$). The corresponding shape variable cross section is defined by

$$R(\alpha_S(\mu), Q/\mu; y) = \int_0^y dy' \frac{1}{\sigma}\frac{d\sigma}{dy'} \quad . \tag{15}$$

The conventional approach for studying shape variables is based on the comparison between data and NLO QCD calculations in the form

$$\begin{aligned} &R(\alpha_S(\mu), Q/\mu; y) = 1 + \alpha_S(\mu) R^{(1)}(y) \\ &+\alpha_S^2(\mu)[R^{(2)}(y) - 2\beta_0 R^{(1)}(y) \ln Q/\mu] \\ &+\mathcal{O}(\alpha_S^3 \ln^2 Q/\mu) \ , \end{aligned} \tag{16}$$

where the perturbative contributions $R^{(1)}(y), R^{(2)}(y)$ have been computed numerically (as described in the previous section) by Kunszt and Nason [29]. Note that, unlike in the case of the fully inclusive quantities , the perturbative terms in eq. (16) are functions of the actual value of the shape variable y. Moreover, in eq. (16) we have explicitly introduced the dependence on the renormalization scale μ. This dependence is formally of NNLO (i.e. $dR/d\ln\mu = \mathcal{O}(\alpha_S^3)$) but it can be numerically large if *i*) μ is very different from the centre-of-mass energy Q (see the $\mathcal{O}(\alpha_S^3 \ln^2 Q/\mu)$ term in eq. (16)), i.e. the natural physical scale of the process, and/or *ii*) the perturbative functions $R^{(n)}(y)$ are large. For these reasons, assuming a well-behaved perturbative expansion, μ is usually set equal to Q and μ variations (typically by a factor of four) around this value are used for estimating the theoretical uncertainty due to uncalculated higher-order contributions. Nevertheless, a more empirical approach is often considered: μ is left as a free parameter and fitted to the data together with α_S.

An updated summary [30,31] of α_S determinations from NLO calculations in e^+e^- annihilation is presented in Fig. 3. All these measurements are pretty consistent and the average value (taking into account experimental and theoretical correlations) for α_S is

$$\alpha_S(M_Z) = 0.119 \pm 0.001(\text{exp.}) \pm 0.006(\text{th.}) \quad . \tag{17}$$

The error is dominated by theoretical uncertainties due to hadronization corrections and higher-order contributions. The non-perturbative hadronization effects are estimated via Monte Carlo event generators by comparing the corresponding results at parton and hadron level. The overall size of these corrections is typically between 5 and 15%. The relative effect among different Monte Carlo generators is instead of the order of few percent and is usually assigned as the corresponding hadronization uncertainty.

Higher-order contributions are estimated from renormalization scale variations. As a matter of fact, the peculiar feature of these QCD tests and α_S determinations to $\mathcal{O}(\alpha_S^2)$ is the following [32]. Far away from the two-jet region, the NLO expression (16) with a renormalization scale $\mu \simeq Q$ gives good fits to the data. On the contrary, reasonable fits in the two-jet region can be achieved only by using renormalization scales μ much smaller than Q (as small as a few GeV!) and values of α_S smaller than those obtained in the multi-jet region.

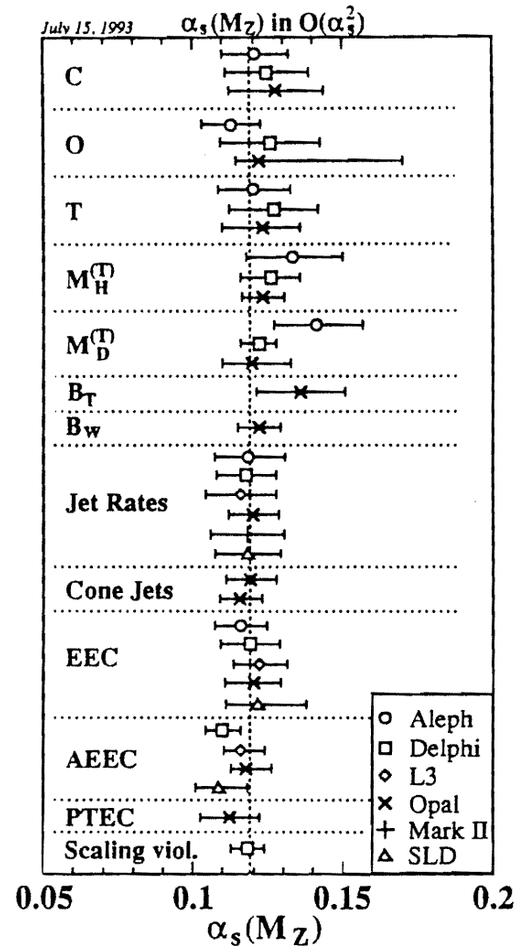

Fig. 3: Compilation of measurements of $\alpha_S(M_Z)$ from event shapes, jet rates, energy correlations and scaling violations, in $\mathcal{O}(\alpha_S^2)$, at LEP and SLC [31].

The reason for this strong scale dependence is that the perturbative functions $R^{(n)}(y)$ in eq. (16) are large in the two-jet region ($y \to 0$). For instance, in the case of thrust the actual calculation gives

$$R(y = 1-T)_T \cong_1 1 - C_F \frac{\alpha_S}{\pi} \ln^2(1-T) + \mathcal{O}(\alpha_S^2 \ln^4(1-T)) \ . \tag{18}$$

The double logarithmic contribution $\alpha_S \ln^2(1-T)$ is due to the bremsstrahlung spectrum of a soft and collinear gluon. Although infrared and collinear singularities cancel in inclusive cross sections upon adding real and virtual contributions, in the two-jet limit real emission is strongly inhibited. The ensuing mismatch of real and virtual corrections generates logarithmically-enhanced terms which spoil the convergence of the perturbative expansion in α_S.

Observables dominated by two-jet configurations are thus affected by a large and *systematic* theoretical uncertainty due to higher-order logarithmic corrections. Reliable predictions can be obtained only computing these corrections and, if possible, resumming them to all orders in α_S.

A detailed understanding of logarithmically enhanced terms now exists for many shape variables [33-37], namely those for which the small-y logarithms $L = \ln 1/y$ *exponentiate* [38]. The shape variable cross section $R(\alpha_S, y)$ can thus be written as follows

$$R(\alpha_S, y) = C(\alpha_S)\Sigma(\alpha_S, L) + D(\alpha_S, y) \,, \qquad (19)$$

where

$$\begin{aligned} C(\alpha_S) &= 1 + \sum_{n=1}^{\infty} C_n \alpha_S^n \\ \ln \Sigma(\alpha_S, y) &= \sum_{n=1}^{\infty}\sum_{m=1}^{n+1} G_{nm}\alpha_S^n L^m = L g_1(\alpha_S L) \\ &+ g_2(\alpha_S L) + \alpha_S g_3(\alpha_S L) + \cdots \,, \end{aligned} \qquad (20)$$

and $D(\alpha_S, y)$ vanishes as $y \to 0$ order-by-order in perturbation theory. The word exponentiation refers to the fact that the terms $\alpha_S^n L^m$ with $m > n+1$ are absent from $\ln R(\alpha_S, y)$, whereas they do appear in $R(\alpha_S, y)$ itself. In the expression (19) the singular $\ln y$ dependence is enterely included in the effective form factor Σ. The function g_1 resums all the *leading* contributions $\alpha_S^n L^{n+1}$, while g_2 contains the *next-to-leading* logarithmic terms $\alpha_S^n L^n$, and g_3 etc. give the remaining *subdominant* logarithmic corrections $\alpha_S^n L^m$ with $0 < m < n$.

Eq. (20) represents an improved perturbative expansion in the two-jet region. Once the functions g_i have been computed, one has a systematic perturbative treatment of the shape distribution throughout the region of y in which $\alpha_S L \lesssim 1$, which is much larger than the domain $\alpha_S L^2 \ll 1$ in which the α_S perturbative expansion (16) is applicable. Furthermore, the resummed expression (20) can be consistently matched with fixed-order calculations. In particular, one can consider the next-to-leading logarithmic approximation (NLLA) as given by the functions g_1 and g_2 and combine them with the order-α_S^2 results in eq. (16) (after subtracting the resummed logarithmic terms in order to avoid double counting), to obtain a prediction (NLLA+$\mathcal{O}(\alpha_S^2)$) which is everywhere at least as good as the fixed-order result, and much better as y becomes small.

Extensive experimental studies based on NLLA+$\mathcal{O}(\alpha_S^2)$ calculations have been carried out during the last two years [39] and further analyses have been presented at this Conference [40]. As expected from the improved theoretical accuracy of these predictions [33], it has been shown that the resummed calculations have a reduced dependence on the renormalization scale and, in particular, remove the need to choose 'unphysical' (very small) renormalization scales in the two-jet region (see, for instance, Fig. 4).

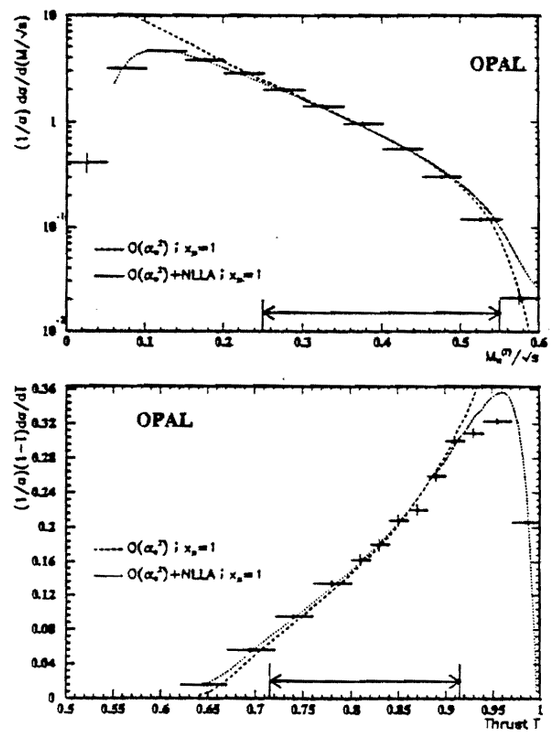

Fig. 4: Measured distributions of heavy jet mass $M_H^{(T)}$ and thrust T, compared with fits to the $\mathcal{O}(\alpha_S^2)$ and to the resummed NLLA+$\mathcal{O}(\alpha_S^2)$ calculations, with a renormalization scale factor $x_\mu \equiv \mu/Q = 1$ in both cases.

A summary of $\alpha_S(M_Z)$ from resummed calculations is given in Fig. 5 [30,31]. The resulting (correlated) average value

$$\alpha_S(M_Z) = 0.123 \pm 0.002(\text{exp.}) \pm 0.005(\text{th.}) \qquad (21)$$

is in good agreement with that obtained from analyses in $\mathcal{O}(\alpha_S^2)$ alone and has a comparable uncertainty. Note however that the theoretical errors are treated differently. All the central values in Fig. 5 refer to the same renormalization scale value $\mu = Q$ and scale uncertainties are evaluated by varying μ by (approximately) a

factor of four around Q. This range includes the best fit values for μ: renormalization scales very different from Q are not only theoretically disfavoured but they also fail in describing the data. Non-perturbative effects are again estimated from Monte Carlo event generators. However, since modern Monte Carlo simulations operate by generating parton configurations of arbitrarily large multiplicity (typically much larger than the maximum of four partons involved at order $\mathcal{O}(\alpha_S^2)$), they are better suited to estimating the hadronization corrections for resummed calculations. In summary, using resummed calculations there is much less freedom to define the central value of α_S and its theoretical uncertainty and a more consistent QCD picture emerges.

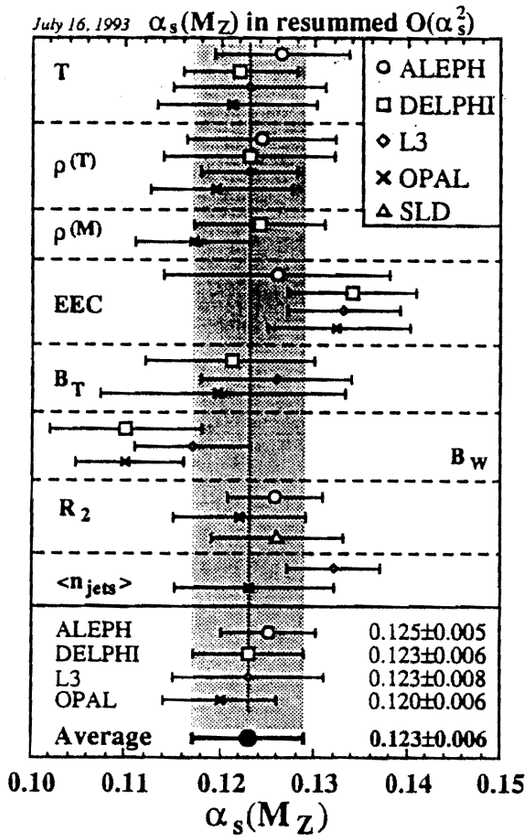

Fig. 5: Summary of measurements of $\alpha_S(M_Z)$ from LEP and SLC, using resummed NLLA+$\mathcal{O}(\alpha_S^2)$ calculations [31].

Jet cross sections

A jet is qualitatively defined as a collimated spray of high-energy hadrons. It is likely to be produced by hard scattering of partons and thus it can be regarded as a universal signal of parton dynamics at short distances. However, in order to perform accurate quantitative studies, one needs a precise definition of jet. Essentially, one has to specify how low-energy particles are assigned to jets.

The standard jet definition in e^+e^- annihilation [41, 29] amounts to introducing a dimensionless resolution variable $y_{ij} = d_{ij}/Q^2$ for every pair (i,j) of particles (jets). Then the particles (jets) with the minimum y_{ij} are merged until a fixed resolution $y_{\rm cut}$ is reached ($y_{ij} > y_{\rm cut}$). The final-state particles in each event are therefore classified in a well defined number of jets, depending on the resolution $y_{\rm cut}$. The main feature of this definition is that the corresponding iterative procedure of clustering type provides an unambiguous and exhaustive assignment of particles to jets.

Several jet clustering algorithms for e^+e^- annihilation are available [29]. Different jet algorithms are specified by the definition of the dimensionful resolution variable d_{ij}. The theoretically favoured resolution variable is [36,42,43]

$$d_{ij}^{(k_\perp)} = \min 2(E_i^2, E_j^2)(1-\cos\theta_{ij}) \ , \qquad (22)$$

where E_i, E_j are the particle (jet) energies in the e^+e^- centre-of-mass frame and θ_{ij} is their relative angle. This resolution variable reduces to the minimal relative transverse momentum $k_{\perp ij}^2$ in the limiting case of small relative angles ($\theta_{ij} \to 0$). For this reason the algorithm is known as $k_\perp$-algorithm.

Let me compare the $k_\perp$-algorithm with an older jet definition as given by the JADE algorithm [41], where the jet resolution variable is essentially the invariant mass $d_{ij}^{(J)} = 2E_iE_j(1-\cos\theta_{ij}) \simeq (p_i+p_j)^2$ of the pair. The resolution variables $d_{ij}^{(k_\perp)}$ and $d_{ij}^{(J)}$ both vanish in the soft limit $E_i, E_j \to 0$ (the two algorithms are thus infrared safe) but they behave differently for small (and finite) particle energies. It follows that they treat soft radiation in a different way. In particular, since $d_{ij}^{(J)}$ depends on the product E_iE_j, the JADE algorithm prefers to merge soft particles first, even if they are far apart in angle. In the case of the $k_\perp$-algorithm, the resolution variable $d_{ij}^{(k_\perp)}$ is instead diagonal with respect to particle energies (i.e. the product E_iE_j is replaced by E_i^2 or E_j^2). Hence, soft particles are merged with the energetic particle closest in angle. The different jet classification is clearly shown by the L3 event reported in Fig. 6 [44]. One can say that the JADE algorithm induces strong *attractive kinematic* (due to the jet definition and independent of the underlying dynamics) *correlations* among soft particles. On the contrary, the $k_\perp$-algorithm, where these correlations are absent, leads to the several advantages: *i*) it avoids a non-intuitive classification of events and an unnatural assignment of particles to jets (soft and wide-angle jets); *ii*) it reduces the size of the non-perturbative corrections due

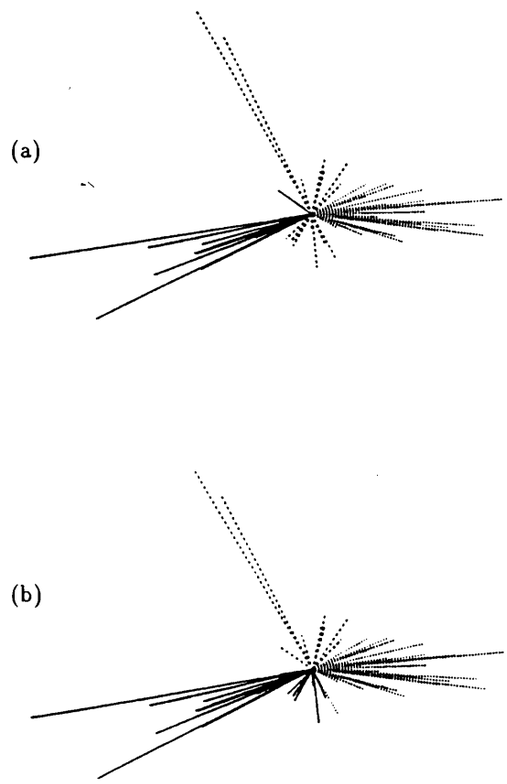

Fig. 6: A 3-jet event as 'seen' by (a) the JADE algorithm and (b) the $k_\perp$-algorithm.

to the hadronization process (since soft particles are merged with the energetic particle closest in angle, soft fragmentation products are likely to be assigned to the 'parent' jet); *iii*) theoretical calculations in perturbative QCD are more reliable, because multi-parton kinematics does not dominate multi-parton dynamics in higher perturbative orders.

The latter point is particularly evident in the small-y_{cut} region, where the QCD perturbative expansion of jet cross sections is dominated by large double logarithmic corrections of the type $\alpha_S^n \ln^m y_{cut} (m \leq 2n)$. These contributions, whose origin is due to the emission of soft and collinear gluons (as for the case of event shapes in the two-jet region), can be resummed to all orders in α_S if jets are defined using the $k_\perp$-algorithm. On the contrary, in the case of the JADE algorithm, the attractive kinematic correlations among soft particles prevent the implementation of the resummation procedure [45].

In the period of about two years since its introduction, the $k_\perp$-algorithm has become popular for both theoretical and experimental applications, including determinations of α_S and studies of jet topology and coherence effects. As an example of these analyses, let me consider the average jet multiplicity $\langle n_{jet} \rangle$ as a function of the jet resolution y_{cut}. This measurement can be considered as an alternative QCD test with respect to the mean multiplicity of hadrons produced in e^+e^- annihilation. An appealing feature of $\langle n_{jet} \rangle$ is that, unlike the hadron multiplicity, it is an infrared safe observable and thus its absolute normalization (and not only its asymptotic increase) is computable in perturbation theory. Moreover, it is highly sensitive to non-abelian effects, i.e. to multiple jet production by gluon cascades. This effect is particularly evident in the small-y_{cut} region where the QCD calculation, to leading accuracy in the double logarithmic expansion parameter $a \equiv (\alpha_S/2\pi) \ln^2 y_{cut}$, predicts

$$\langle n_{jet} \rangle - 2 \underset{y_{cut} \ll 1}{\simeq} C_F a \left[1 + \frac{1}{12} C_A a + \frac{1}{360} C_A^2 a^2 + \cdots \right] . \tag{23}$$

Note that in this approximation the deviation of eq. (23) from the double logarithmic behaviour $\alpha_S \ln^2 y_{cut}$ is enterely due to non-abelian (i.e. proportional to powers of the gluon charge $C_A = N_c$) contributions. The QCD predictions for $\langle n_{jet} \rangle$ in NLLA+$\mathcal{O}(\alpha_S^2)$ have been succesfully tested by the L3 and OPAL Collaborations [39] (see Fig. 7).

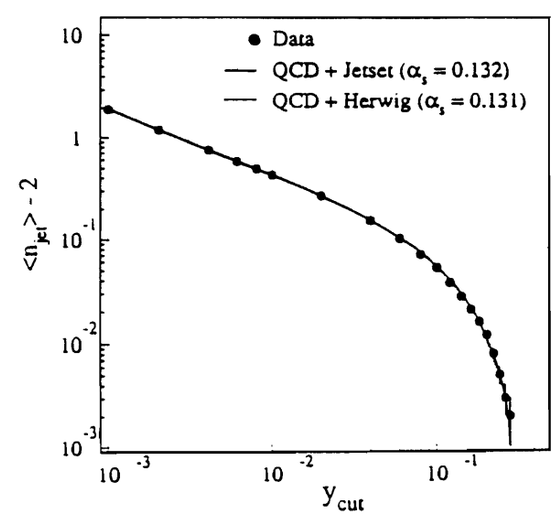

Fig. 7: L3 data on the average jet multiplicity $\langle n_{jet} \rangle$ compared with NLLA+$\mathcal{O}(\alpha_S^2)$ predictions.

Many more studies of jet properties in e^+e^- annihilation have been reviewed in Refs. [44,46,47]. I shall come back to the issue of jet definition in the following sections.

Jet physics in hadron-hadron collisions

Perturbative QCD predictions for hadron-hadron

collisions need an extra input with respect to e^+e^- annihilation: the parton densities of the incoming hadrons to be convoluted with hard-scattering cross sections. The present knowledge of parton densities is reviewed elsewhere at this Conference [1]. For the purpose of the following presentation, let me just mention that, waiting for new exciting results from HERA [2], a new generation of NLO parton densities was born in the last year [48]. They incorporate new and accurate data in the range $x \sim 10^{-2}$ from the NMC [49] and CCFR [50] experiments and their main difference with respect to previous parton densities is in the increase (about 20%) of the sea quark distributions in the small-x domain ($0.01 \lesssim x \lesssim 0.08$).

Cone algorithms

In hadron-hadron collisions jets are usually defined in terms of cone algorithms: a jet consists of all the particles whose momenta lie inside a cone of radius R in the pseudorapidity-azimuth space. To be definite, I shall consider the cone algorithm outlined in the so-called 'Snowmass Accord' [51]. Following the Snowmass Accord a particle of transverse energy E_{Ti}, pseudorapidity $\eta_i = -\ln(\tan\theta_i/2)$ and azimuth ϕ_i (with respect to the direction of the colliding hadrons) belongs to the jet if

$$\sqrt{(\eta_i - \eta_J)^2 + (\phi_i - \phi_J)^2} < R \ , \qquad (24)$$

where the kinematic variables of the jet are defined by

$$E_{TJ} = \sum_{i \in \text{cone}} E_{Ti} \ , \quad \{\eta_J, \phi_J\} = \sum_{i \in \text{cone}} \{\eta_i, \phi_i\} E_{Ti}/E_{TJ} \ , \qquad (25)$$

To a good approximation, this cone algorithm is implemented in the experimental analyses by the CDF and D0 Collaborations [52,53]. In the following I shall discuss the comparison between NLO QCD predictions [54,55] and Tevatron data. In particular, I shall address some points which require further investigations and that I consider relevant for the present and future understanding of jet physics in hadron collisions. These points refer to: *i*) the role of underlying-event effects; *ii*) the merging issue in the case of overlapping cones; *iii*) the size of non-perturbative fragmentation contributions.

Jet studies in NLO QCD

During the last three years, detailed studies of jet properties have been carried out by the CDF Collaboration at the Fermilab Tevatron $p\bar{p}$ collider. Also the D0 Collaboration has joined these analyses in the last year, extending the covered angular region up to $|\eta| < 3$. The comparison between NLO QCD predictions [54] and Tevatron data [56] for the one-jet inclusive cross section is shown in Fig. 8. These results are for $\sqrt{s} = 1.8$ TeV and are averaged over a proper rapidity range with a cone of size $R = 0.7$†. Note that the NLO QCD calculation provides an absolute prediction for the cross section: the agreement with data over nearly ten orders of magnitude is remarkable. The theoretical uncertainty of the calculation is estimated to be about 15% [57]. This estimate relies on the dependence on both the renormalization scale μ (the 'physical' range $E_T/4 \leq \mu \leq E_T$ is considered) and the parton densities.

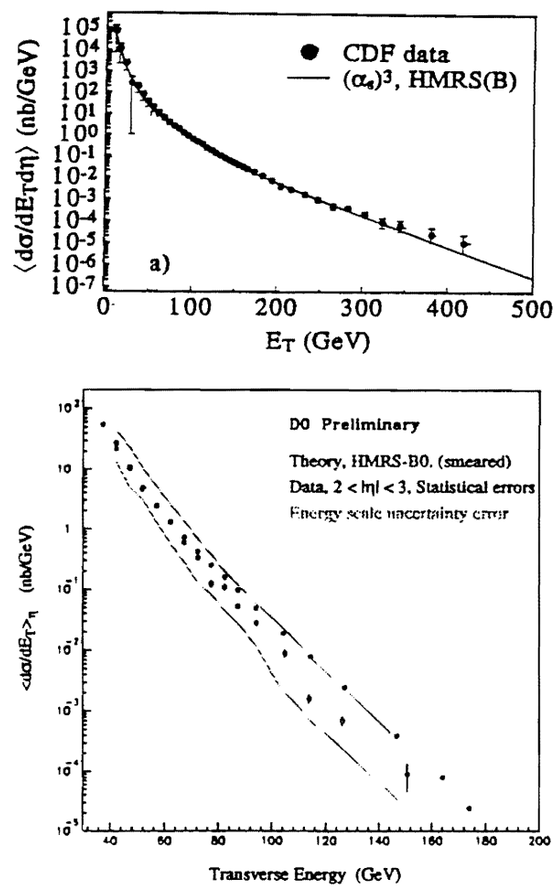

Fig. 8: The one-jet inclusive cross sections measured by CDF ($0.1 \leq |\eta| \leq 0.7$) and D0 ($2 \leq |\eta| \leq 3$), and compared with NLO QCD predictions.

An independent source of uncertainty for the perturbative QCD prediction is represented by the underlying event, i.e. low-$p_\perp$ fragments produced by soft interactions of the spectator partons in the colliding hadrons. The effect of the underlying event on the cross section in Fig. 8 is estimated to be small [57], at least

†The value $R = 0.7$ for the cone size is that preferred by the NLO QCD calculation [57] in order to minimize the theoretical uncertainty due to higher-order contributions.

for $E_T > 50\,\mathrm{GeV}$. Nonetheless it can contribute substantially to other jet measures. In order to discuss this point, let me consider the measurement of scaling violations in jet cross sections.

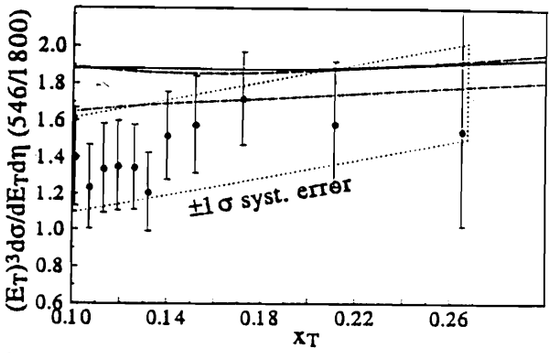

Fig. 9: Ratio of the dimensionless distributions $E_T^3 d\sigma/dE_T$ at $\sqrt{s} = 546\,\mathrm{GeV}$ and 1800 GeV (the dotted box represents the experimental systematic uncertainty). The solid and dashed curves are NLO predictions corresponding to different parton densities. The dot-dashed curve is the NLO prediction after the over-correction for the underlying-event contribution.

The CDF Collaboration [58] has measured the dimensionless inclusive distribution $E_T^3 d\sigma/dE_T$ at two different centre-of-mass energies, $\sqrt{s} = 1800\,\mathrm{GeV}$ and 546 GeV. According to the naive parton model, each of these distributions is a function of the sole scaling variable $x_T = 2E_T/\sqrt{s}$. Perturbative QCD predicts an additional dependence (scaling violation) on E_T (more precisely, E_T/Λ) or, equivalently, on $\sqrt{s}$ at fixed x_T. The data, reported in Fig. 9, clearly show scaling violations. However, in the low-x_T region, they disagree at the level of two standard deviations with the NLO QCD predictions. A tentative explanation of this disagreement has been proposed in Ref. [59]. It is based on the treatment of the underlying-event corrections. Experimental studies of minimum bias events [60] suggest that the underlying event generates a distribution of transverse energy which is almost uniform in the variables η and ϕ. The CDF Collaboration determines this underlying event contribution at each $\sqrt{s}$ by measuring the E_T density at large distance (in the $\eta-\phi$ plane) from the jet axis, the so-called 'pedestal' of the jet. Then an equivalent energy density is subtracted from the jet core in order to correct the data and compare them with the theory. The main observation in Ref. [59] is that the energy density measured in the pedestal is about a factor of two larger than the corresponding energy density measured in minimum bias events. Therefore a substantial contribution to the pedestal height can be consistently attributed to soft QCD radiation associated to the jet activity. Since QCD radiation is already accounted for in the NLO calculation, this implies that the current data may have been over-corrected. Actually, applying the corresponding over-correction to the theoretical prediction, the discrepancy between data and theory is reduced at the level of about one standard deviation (Fig. 9). While this improvement is perhaps not overwhelming, I think that the problem addressed is relevant and that further studies of the underlying-event contributions to jet physics are clearly warranted. For instance, one can try to compare cone jets produced in hadron collisions with similarly defined jets in e^+e^- annihilation (where the underlying event is absent). A first step towards this direction has been already performed by the OPAL Collaboration [61].

Another open question about jets in hadron collisions concerns the merging issue. In fact, at least in their simplest formulation, cone algorithms are not unambiguously defined. In the case of events with many final-state particles, the constraint (24) can be satisfied by configurations where individual particles are members of more than one jet, i.e. the cones are found to overlap. Hence, the cone algorithm must be supplemented with additional conditions able to specify how particles in the overlapping region have to be assigned to jets. This ambiguity has only a small effect on highly inclusive quantities (like the one-jet inclusive cross section) but it can have a large numerical impact on the properties of multi-jet configurations and on the detailed internal structure of jets.

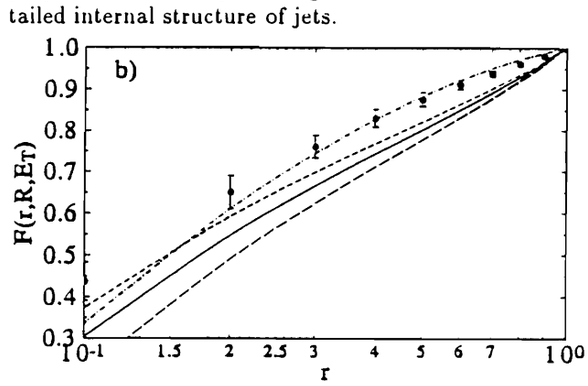

Fig. 10: CDF data on the transverse-energy profile of the jets compared with the $\mathcal{O}(\alpha_S^3)$ calculations. The dashed lines delimit the region spanned by the theoretical predictions for the original jet algorithm of the 'Snowmass Accord'. The dot-dashed curve corresponds to the prediction for the modified algorithm with $R_{\mathrm{sep}} = 1.3R$.

The CDF Collaboration has started to investigate the internal structure of jets by studying their transverse-energy profile [62]. Given a sample of jets of transverse energy E_T defined with a cone radius R, the average fraction $F(r, R, E_T)$ of transverse energy that lies inside an inner cone of radius $r < R$ (concentric

with the jet-defining cone) has been measured. The data reported in Fig. 10 refer to $E_T = 100$ GeV and $R = 1.0$. While there is a crude agreement between the theoretical prediction in $\mathcal{O}(\alpha_S^3)$ and the experimental result, the latter suggests that the observed jets have less energy fraction near the edge of the cone. A tentative explanation of this discrepancy, as proposed in Ref. [57], refers to the merging issue. According to the condition (24) for the 'Snowmass Accord', in the $\mathcal{O}(\alpha_S^3)$ calculation two partons are merged into a single jet up to the limiting configuration in which they have equal transverse energy and a relative distance $2R$ in the pseudorapidity-azimuth space. On the other side, because of the supplementary conditions needed in the experimental practice to disentangle overlapping cones, the CDF algorithm is likely to recognize the above limiting configuration as two distinct jets. In order to simulate better the experimental jet algorithm, an extra constraint can be introduced in the theoretical calculation: two partons are no longer merged into a single jet if their distance $R_{ij} = \sqrt{(\eta_i - \eta_j)^2 + (\phi_i - \phi_j)^2}$ is larger than a fixed value $R_{\rm sep}$. As shown in Fig. 10, the $\mathcal{O}(\alpha_S^3)$ prediction turns out to be consistent with the data for $R_{\rm sep} = 1.3R$. This argument offers a reasonable explanation of the observed energy profile of the jet. However it may be considered as an *ad hoc* explanation and raises the question whether the merging issue has to be reconsidered for each jet observable.

The jet studies discussed so far and many others reported at this Conference [56] enhance our confidence in perturbative QCD in the large E_T regime and, at the same time, hint at possible problems in the present understanding of the fine structure of hadronic jets. In particular, it emerges that future developments in the field are strictly linked to the definition and the details of the jet-finding algorithm.

Alternative jet definitions

Clustering algorithms of the type used in e^+e^- annihilation allow an unambiguous and exhaustive assignment of particles to jets. Therefore it may be worthwhile considering their use also for hadron-hadron collisions. The generalization to hadron collisions of e^+e^- clustering algorithms is by no means trivial, because one has to face the problem of dealing with the soft remnants of the incoming hadrons and factorize them from high-$p_\perp$ jets produced by hard scattering of partons. As proposed in Ref. [63], resolution variables of transverse momentum type are particularly suitable for this purpose and, actually, a $k_\perp$-clustering algorithm for hadron collisions has been set up in Refs. [64,65]. Following this algorithm, the observed final state particles are merged into jets or factorized into the beam remnants according to which of the resolution variables $d_{ij} = \min(E_{Ti}^2, E_{Tj}^2)\sqrt{(\eta_i - \eta_j)^2 + (\phi_i - \phi_j)^2}$ (the longitudinally boost-invariant generalization of the minimal relative transverse momentum) and $d_{iB} = E_{Ti}^2$ (the transverse momentum square with respect to the incoming hadron direction) is the smallest one.

The $k_\perp$-clustering algorithm may offers some advantages with respect to cone algorithms. The merging issue is indeed avoided by definition. Moreover, the $k_\perp$-algorithm can be more stable with respect to non-perturbative contributions (either from the underlying event or from fragmentation smearing) and higher-order perturbative corrections [64-66].

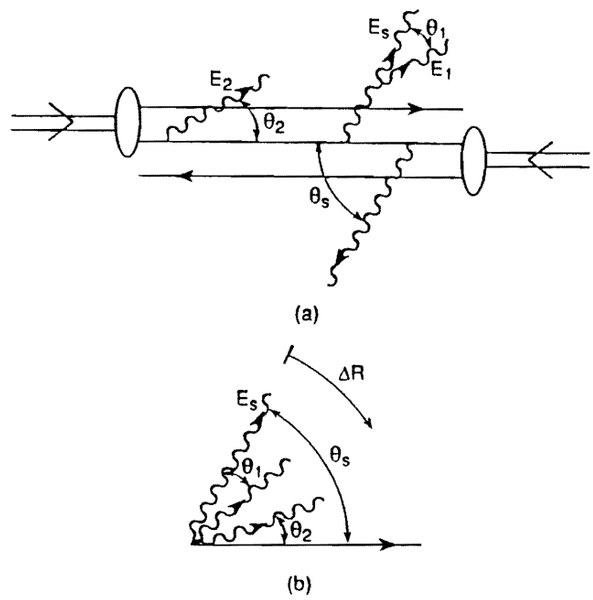

Fig. 11: a) Soft gluon emission accompanying a hard-scattering process and b) the corresponding angular configuration.

In order to illustrate this point and to compare (at a qualitative level) the two algorithms, let us consider the case in which two hard partons (with energy E_S and scattering angle θ_S) are produced by $q\bar{q}$-scattering (Fig. 11*a*). We can then discuss how two soft ($E_1, E_2 \ll E_S$) and collinear ($\theta_1, \theta_2 \ll \theta_S$) gluons p_1 and p_2, produced respectively by final-state fragmentation and initial-state radiation, are assigned to jets by different algorithms. Using a $k_\perp$-resolution variable, the gluon p_1 is clustered with the hard parton E_S and the gluon p_2 is assigned to the beam jet. Instead, in a cone algorithm both p_1 and p_2, or p_1 or neither of them are included in the hard jet depending on the actual values of the cone radius R and the scattering angle θ_S (Fig. 11*b*). We see that the $k_\perp$-algorithm works as a variable-radius cone algorithm, and the effective radius depends on the kinematics (and the colour flow) of the

hard-scattering subprocess. Therefore, we may argue that the $k_\perp$-algorithm corresponds better to the QCD expectation that soft hadrons produced *coherently* by the fragmentation of hard partons should be naturally assigned to the jet of the energetic parton nearest in angle, independently of the actual value of its angular distance. Moreover, on the perturbative side it has been found [65] that the $k_\perp$-algorithm gives in $\mathcal{O}(\alpha_S^3)$ approximately (within 15%) the same one-jet inclusive cross section as for the cone algorithm with a cone radius $R \simeq 0.7$. This cone size is that which minimizes (a posteriori) the theoretical uncertainty in the $\mathcal{O}(\alpha_S^3)$ calculation for the cone algorithm. This coincidence may well be a numerical accident but, at least, it offers some physical intuition on the 'optimal' radius $R \simeq 0.7$. After all, the fact that one gets, for free, jet cross sections with a reduced (if estimated as for the cone algorithm) theoretical uncertainty, is a promising feature of the $k_\perp$-algorithm. In conclusion, I think that future theoretical and experimental studies of different jet algorithms can help for a deeper understanding of jet properties. This issue is even more relevant for DIS processes, which, in a sense, are intermediate between e^+e^- annihilation and hadron-hadron collisions.

Jets in *ep* collisions

A large number of new QCD analyses have been reported at this Conference [2,67,68] by the experiments at the *ep* collider HERA at DESY/Hamburg. For this reason this section is mostly devoted to HERA studies of hadronic final states in photoproduction and DIS.

Photoproduction

Beam electron scattering at small angles in *ep* colliders is an intense source of quasi-real (with invariant mass $Q^2 \sim 0$) photons, and can be used for studying photoproduction processes. In the case of high-energy photoproduction, QCD predicts [69] a large contribution coming from hard parton scattering via two different mechanisms, the so-called *direct* and *resolved* mechanisms (Fig. 12). In the first case the photon couples directly to quarks and the coupling is pointlike. In the second case, the photon participates in the scattering process through its hadronic component, described in terms of the photon structure function. The photon structure function consists in turn of two different terms: a hadron-like contribution, usually described in terms of the vector meson dominance model, and a partonic contribution which is controlled by perturbative QCD. Both the direct contribution and the short distance behaviour of the photon structure function are calculable in perturbation theory. In particular, perturbative QCD predicts [69] that the partonic content of the structure function increases like $\ln p_\perp^2/\Lambda^2$ ($p_\perp$ being the transverse momentum of the scattered parton) thus dominating jet production at high energies.

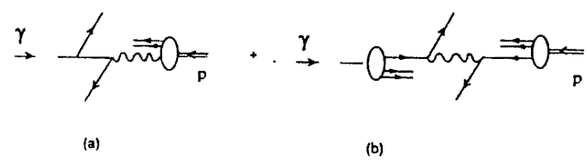

Fig. 12: a) Direct and b) resolved contributions to the photoproduction process.

High-$p_\perp$ jets (defined with a cone algorithm), produced in the photoproduction regime with $Q^2 < 4\,\mathrm{GeV}^2$ and photon-proton centre-of-mass energy between 100 and 300 GeV, have been observed by the H1 and ZEUS Collaborations at HERA [70]. The one-jet inclusive cross section measured by H1 is reported in Fig. 13 and compared with the corresponding Monte Carlo simulation of the event generator PYTHIA (based on leading order QCD) [71]. In the high-$p_\perp$ region ($p_\perp > 10\,\mathrm{GeV}$) the Monte Carlo predictions are consistent with the data. In particular, if only the direct contribution is considered, the predicted cross section falls short of the measured one by at least an order of magnitude.

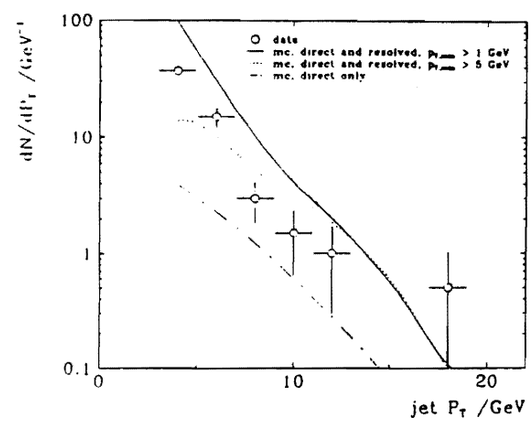

Fig. 13: H1 data on the inclusive p_T distribution of jets compared with the predictions of the PYTHIA Monte Carlo program (solid and dotted lines). The dot-dashed line is the prediction if the resolved photon contribution is excluded.

An independent and direct evidence for the resolved photon component comes from the study of the event topologies. Direct and resolved photon contributions have indeed a different jet signature (Fig. 12): while the direct component leads to a (2+1)-jet final state (two high-$p_\perp$ jets and a remnant jet along the proton direction), an additional remnant jet (along the photon direction) is produced by the resolved mechanism. The

substantial amount of hadronic energy observed in the photon direction (Fig. 14) clearly shows the presence of the resolved photon subprocess.

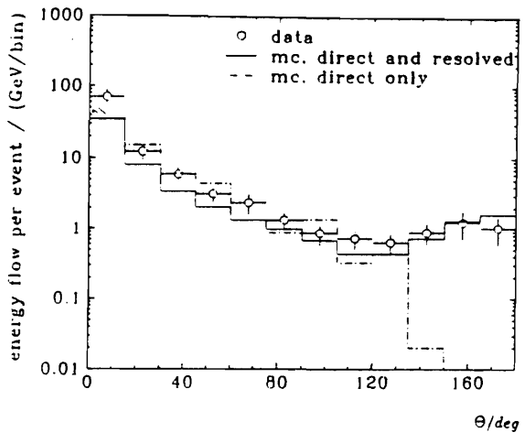

Fig. 14: H1 data on the energy flow versus the polar angle Θ ($\Theta = 180°$ is the photon direction). The full line represents the Monte Carlo simulation for the resolved and direct processes, whereas the dot-dashed line gives the prediction for the direct process only.

The comparison between photoproduction data and QCD predictions has been performed so far at a semi-quantitative level. With the increased statistics expected from the next HERA run, more detailed quantitative tests of QCD will be possible. In particular, using the NLO QCD calculations[‡] [72,73] which have become available in the last few months, accurate information on the photon structure function can be extracted from the data.

Final states in DIS

In 1992, most of the HERA data on DIS have been collected in the kinematic range of moderate transferred momentum Q^2 ($4\,\mathrm{GeV}^2 < Q^2 < 100\,\mathrm{GeV}^2$) and low Bjorken x ($10^{-4} < x < 10^{-2}$) with an average value $\langle W \rangle \sim 100\,\mathrm{GeV}$ of the $\gamma^* p$ centre-of-mass energy. QCD studies of hadronic final states have been concentrated on the comparison with Monte Carlo event generators. The QCD based Monte Carlo models which have been considered are LEPTO PS, LEPTO ME+PS, ARIADNE and HERWIG [71]. LEPTO PS is a parton shower Monte Carlo which generates parton cascades to leading logarithmic accuracy in perturbative QCD. The amount of radiation produced in the final state by the showering process is controlled by the maximum kinematic scale chosen for the initial-state QCD evolution. The two different options Q^2 and $W^2 = Q^2(1-x)/x$ for this scale have been extensively studied: in the small-x regime they represent two extreme limiting cases ($Q^2 \ll W^2$). More detailed dynamics information is instead contained in the other Monte Carlo models. LEPTO ME+PS includes the complete leading-order QCD matrix element, while the latter is approximated in ARIADNE and HERWIG respectively by a colour dipole and by taking into account QCD coherence. As a result, in these improved models the initial-state parton shower evolves up to a dynamical scale roughly proportional to the transverse momentum square of the quark scattered by the the electroweak current.

Fig. 15 shows the hadronic-energy distribution as a function of the pseudorapidity in the HERA laboratory frame. The origin $\Delta\eta = 0$ in Fig. 15 is set at the pseudorapidity value corresponding to the struck quark in the naive parton model. The data clearly show that the target fragmentation region ($\Delta\eta > 0$) is filled up by initial-state QCD radiation. Moreover, the comparison with the Monte Carlo simulations witnesses the inability of the simple parton shower models to reproduce the data. Depending on the choice Q^2 or W^2 for the evolution scale, LEPTO PS gives too little or too much radiation from the initial state. On the contrary, LEPTO ME+PS, ARIADNE and HERWIG give a reasonable description of the measured energy flow.

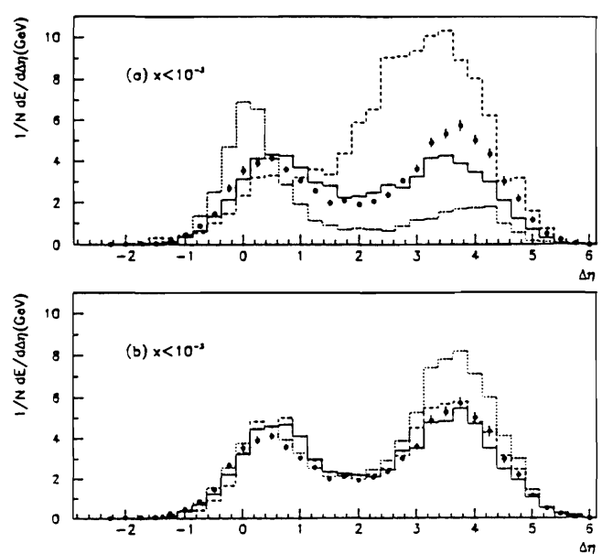

Fig. 15: The hadronic-energy distribution versus the pseudorapidity $\Delta\eta$ in DIS events. The ZEUS data points are compared with Monte Carlo simulations: (a) LEPTO ME+PS (full line), LEPTO PS with evolution scale W^2 (dashed line) or Q^2 (dotted line); (b) ARIADNE (full line), HERWIG (dashed line), HERWIG with a model for the soft underlying event (dotted line).

[‡]Note that at present there is a pretty large numerical discrepancy (between 40 and 80%) among different calculations [72] of the resolved contribution.

Similar conclusions can be drawn from the analysis of other global event characteristics [74]. The simple tuning of the kinematic parameters in the parton shower model fails to explain the HERA data. An overall consistency with the experimental results is instead achieved by the Monte Carlo generators in which the parton shower is matched with hard QCD radiation.

The first evidence of multi-jet structures in DIS has been reported recently by the E665 Collaboration [75]. At HERA, multi-jets events are clearly visible and both the H1 and ZEUS Collaborations have started detailed analyses of jet production rates [68,76]. The jet algorithm used so far is a modified version [77] of the JADE algorithm for e^+e^-. In this algorithm the dimensionless resolution variable y_{ij} is defined by rescaling the invariant mass $d_{ij}^{(J)} = 2E_iE_j(1-\cos\theta_{ij})$ (i.e. the dimensionful resolution variable used by the JADE algorithm in e^+e^-) with the centre-of-mass energy square W^2 of the final-state hadronic system ($y_{ij} = d_{ij}^{(J)}/W^2$). Moreover, in order to deal with the remnant of the incoming proton, the clustering procedure considers not only the observed final-state particles but also an additional pseudoparticle carrying the missing (i.e. lost in the beam pipe) longitudinal momentum of the event.

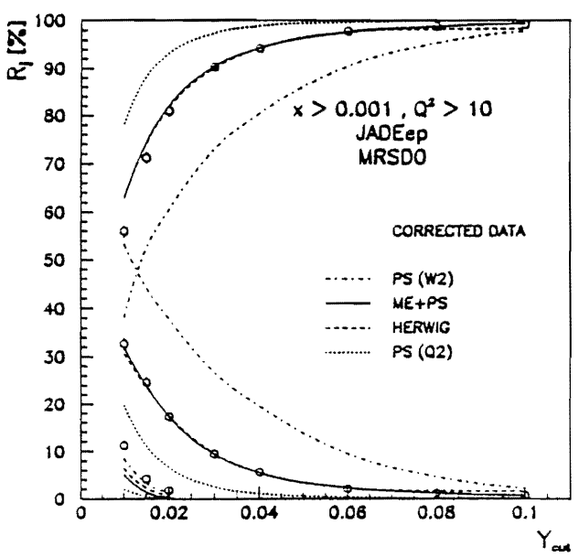

Fig. 16: ZEUS data on the jet rates R_j ($j = (0+1)+(1+1), j = (2+1), j = (3+1)$ reading downwards) compared with Monte Carlo predictions.

Fig. 16 shows the $(n+1)$-jet rates (the notation $n+1$ refers to n final-state jets plus the proton remnant) as reported at this Conference by the ZEUS Collaboration [68]. The data are well described by the improved Monte Carlo models (simple parton showers fail again), but additional analyses on the size of the hadronization corrections and on the sensitivity to different parton densities are necessary before a detailed comparison with the available NLO QCD calculations [78] can be performed. In view of the discussion developed in the previous sections, also theoretical and phenomenological investigations of different jet algorithms are desiderable [63,79]. Certainly, more quantitative QCD studies and results, such as determinations of α_S, will come in the near future.

Summary of α_S determinations

Many theoretical and experimental analyses have been recently devoted to the determination of the strong coupling constant α_S. In Table 1 I have reported an updated version of the compilation of α_S determinations presented by S. Bethke at the '92 Dallas Conference [47]. The α_S values in Table 1 which differ from those in Ref. [47] have been discussed in the previous sections. The main quantitative differences are related to a sizeable decrease of α_S as extracted from the total cross sections in e^+e^- annihilation below and at the Z^0 peak. In the first case, the reduction in the central value of α_S is due to the new theoretical input (the consistent treatment of electroweak radiative corrections) in Haidt's analysis [11]. In the second case, α_S has decreased because of the improved statistics: the central value[§] of α_S is one standard deviation smaller than the previous one.

The only result in Table 1 which is derived from low-energy phenomenology and, hence, non-perturbative techniques is that obtained from the mass splitting of the charmonium states [80], calculated using lattice gauge theory (LGT). The sources of the theoretical uncertainty in this α_S determination have been discussed elsewhere [81,82] and, in particular, the very small theoretical error estimated in [80] has been questioned [81].

All the other results in Table 1 come from high-energy phenomenology (jet physics). As theoretical input, they use QCD perturbation theory plus an estimate of non-perturbative corrections.

The values of α_S, as a function of the energy scale Q, are compared with the QCD prediction of a running coupling in Fig. 17. The energy dependence of the α_S results from *jet physics* is distinct, and is in very good agreement with the QCD running. Therefore it is meaningful to evolve (according to perturbative QCD) all the results to $\alpha_S(M_Z)$. A significant subset of these values is shown in Fig. 18. This subset is chosen by considering a single α_S value for each relevant process and/or en-

[§]The value reported in Table 1 is the average of the two determinations [15,16] discussed in the second section.

Table 1: Summary of measurements of α_s.

Process	Q [GeV]	$\alpha_s(Q)$	$\alpha_s(M_{Z^0})$	$\Delta\alpha_s(M_{Z^0})$ exp.	$\Delta\alpha_s(M_{Z^0})$ theor.	order of perturb.
GLS [CCFR]	1.73	0.32 ± 0.05	0.115 ± 0.006	0.005	0.003	NNLO
R_τ [world]	1.78	0.36 ± 0.05	0.122 ± 0.005	0.002	0.004	NNLO
DIS [ν]	5.0	$0.193 \pm^{0.019}_{0.018}$	0.111 ± 0.006	0.004	0.004	NLO
DIS [μ]	7.1	0.180 ± 0.014	0.113 ± 0.005	0.003	0.004	NLO
$c\bar{c}$ mass splitting	5.0	0.174 ± 0.012	0.105 ± 0.004	0.000	0.004	LGT
$J/\Psi, \Upsilon$	10.0	$0.167 \pm^{0.015}_{0.011}$	$0.113 \pm^{0.007}_{0.005}$	0.001	$\pm^{0.007}_{0.005}$	NLO
e^+e^- [σ_{had}]	35.0	0.146 ± 0.030	0.124 ± 0.021	–	–	NLO
e^+e^- [ev. shapes]	35.0	0.14 ± 0.02	0.119 ± 0.014	–	–	NLO
e^+e^- [ev. shapes]	58.0	0.130 ± 0.008	0.122 ± 0.007	0.003	0.007	NLO
e^+e^- [ev. shapes]	58.0	0.132 ± 0.008	0.124 ± 0.007	0.004	0.006	resum.
$p\bar{p} \to b\bar{b}X$	20.0	$0.138 \pm^{0.028}_{0.019}$	$0.109 \pm^{0.016}_{0.012}$	$\pm^{0.012}_{0.007}$	$\pm^{0.011}_{0.010}$	NLO
$p\bar{p} \to W$ *jets*	80.6	0.123 ± 0.025	0.121 ± 0.024	0.017	0.016	NLO
e^+e^- [scal. viol.]	91.2	0.118 ± 0.005	0.118 ± 0.005	0.001	0.005	NLO
$\Gamma(Z^0 \to$ had.)	91.2	0.122 ± 0.009	0.122 ± 0.009	0.007	$\pm^{0.005}_{0.004}$	NNLO
Z^0 [ev. shapes]	91.2	0.119 ± 0.006	0.119 ± 0.006	0.001	0.006	NLO
Z^0 [ev. shapes]						
SLD	91.2	0.126 ± 0.007	0.126 ± 0.007	0.004	0.006	resum.
ALEPH	91.2	0.125 ± 0.005				resum.
DELPHI	91.2	0.123 ± 0.006				resum.
L3	91.2	0.124 ± 0.009				resum.
OPAL	91.2	0.120 ± 0.006				resum.
LEP *Average*	91.2		0.123 ± 0.006	0.002	0.005	resum.

ergy range[¶]. The measurements from jet physics agree quite well with each other, within their overall errors, and the resulting *weighted average* (leaving out the result from charmonium mass splitting) is

$$\alpha_S(M_Z) = 0.118 \ . \tag{26}$$

While it is straightforward to quote the average value, the uncertainty on $\alpha_S(M_Z)$ is difficult to define since the errors on the various α_S determinations are mainly of theoretical nature and, hence, highly correlated[‖]. Here I present two different estimates of the uncertainty on α_S

$$\Delta\alpha_S(M_Z) = \pm 0.005 \quad \text{(optimistic)} \ , \tag{27}$$

$$\Delta\alpha_S(M_Z) = \pm 0.007 \quad \text{(conservative)} \ . \tag{28}$$

The optimistic view derives from considering that the errors on each α_S determination from jet physics, reported in Table 1 and Fig. 18, are reliably estimated. Thus the optimistic value in (27) is equal to the smallest of these errors. No further reduction of the error coming from the weighting procedure has been considered, because of the strong (theoretical) correlations among the various uncertainties. The conservative attitude follows from arguing that the theoretical errors on the α_S values in Fig. 18 may have been underestimated [81]. Possible sources of this underestimate are, for instance, hadronization corrections in e^+e^- annihilation and heavy-quark mass effects in DIS. Despite this residual ambiguity in the error assignment, the world

[¶]In the case of e^+e^- annihilation, the errors on the α_S determinations from the total cross sections are larger than those from the event shapes at the same energy. Therefore, the fact of including two values of α_S from e^+e^- annihilation below and at the Z^0 peak does not change the conclusions reported in the following.

[‖]The fit of the α_S values in Fig. 18 gives $\chi^2 = 3.7$ for 8 d.o.f. In the case of gaussian errors, the corresponding uncertainty on $\alpha_S(M_Z)$ would be $\Delta\alpha_S(M_Z) = \pm 0.003$.

average value of $\alpha_S(M_Z)$ is now very stable [47,81,83] and the consistency of the α_S determinations from all the available experiments provides a remarkable quantitative test of QCD.

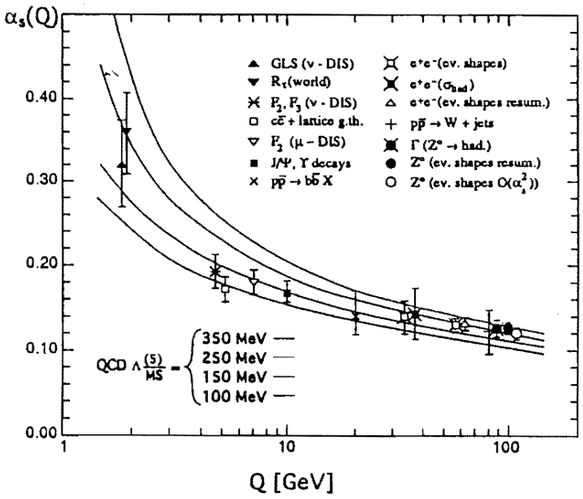

Fig. 17: Summary of $\alpha_S(Q)$. The lines indicate the QCD predictions in NNLO for four different values of $\Lambda^{(5)}_{\overline{MS}}$.

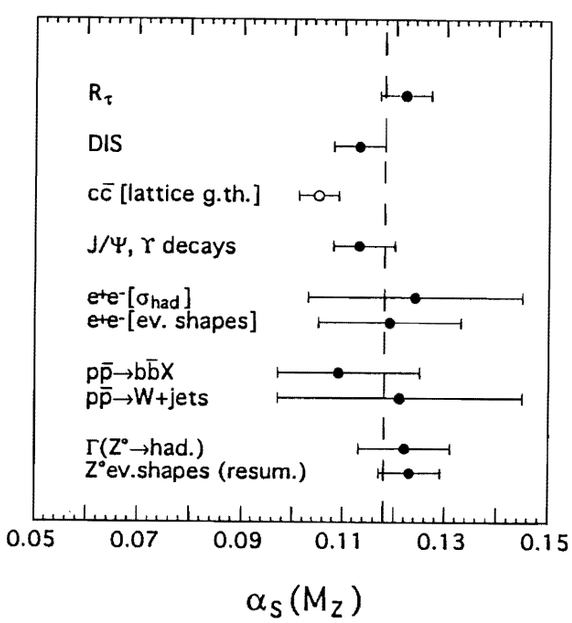

Fig. 18: Summary of measurements of $\alpha_S(M_Z)$.

Outlook

In the last few years, with the advent of high-energy and high-precision experiments and accurate theoretical calculations, detailed tests of QCD have become possible. The results described in this brief review and many others presented at this Conference witness the very good agreement between (NLO) perturbative QCD predictions and jet physics data. More importantly, they have opened new prospects in hadronic physics: hadronic jets are no longer just an observed (and predicted) phenomenon but rather a powerful tool for investigating the dynamics of quark and gluons at short distances.

Future developments in the field require progress in the theory (calculations beyond NLO) as well as accurate theoretical and experimental studies of multijet ($n \geq 3$) structures. Moreover, with the increasing centre-of-mass energy available at present and future hadron colliders, a new kinematic region, the region of small values of the Bjorken variable x, is now opening up. Our understanding of perturbative QCD in this regime has still to be improved, as, possibly, already signalled by the difficulties [84,85] in explaining the data on direct-photon and heavy-flavour production [56,86]. The forthcoming HERA results will play a major role in exploring this kinematic region. Certainly, multijet physics and small-x physics have to be regarded as the new frontiers of QCD.

Acknowledgements

I am grateful to the many colleagues who provided me with detailed information about their results. In particular, I wish to thank G. Altarelli, E. Berger, S. Bethke, W. Buchmüller, S. Ellis, P. Nason, D. Schaile, D. Ward, and B. Webber for many useful discussions.

References

1. W. Buchmüller, plenary talk at this Conference; R.G. Roberts, review talk in the parallel session on *Structure Functions* at this Conference.
2. See the plenary talks by A. De Roeck and R. Klanner at this Conference.
3. E. Hughes, plenary talk at this Conference.
4. F.T. Tkachov, Phys. Lett. 100B (1981) 65; K.G. Chetyrkin and F.T. Tkachov, Nucl. Phys. B192 (1981) 159.
5. S.G. Gorishny, A.L. Kataev and S.A. Larin, Phys. Lett. 259B (1991) 144; L.R. Surguladze and M.A. Samuel, Phys. Rev. Lett. 66 (1991) 560.
6. B.A. Kniel and J.H. Kühn, Phys. Lett. 224B (1989) 229, Nucl. Phys. B329 (1990) 557.

7. K.G. Chetyrkin and A. Kwiatkowski, Phys. Lett. 305B (1993) 285; K.G. Chetyrkin, Phys. Lett. 307B (1993) 169; K.G. Chetyrkin, J.H. Kühn and A. Kwiatkowski, preprint TTP 93-15, submitted to this Conference.

8. S.A. Larin, F.V. Tkachov and J.A.M. Vermaseren, Phys. Rev. Lett. 66 (1991) 862; S.A. Larin and J.A.M. Vermaseren, Phys. Lett. 259B (1991) 345.

9. E.B. Zijlstra and W.L. van Neerven, Nucl. Phys. B383 (1992) 525, Phys. Lett. 297B (1992) 377.

10. T. Matsuura, R. Hamberg and W.L. van Neerven, Nucl. Phys. B359 (1991) 343; W.L. van Neerven and E.B. Zijlstra, Nucl. Phys. B382 (1992) 11.

11. D. Haidt, to appear in *Precision Tests of the Standard Electroweak Model*, edited by P. Langacker (World Scientific, 1993).

12. D. Bardin et al., preprint CERN-TH.6643/92.

13. Particle Data Group, Review of Particles Properties, Phys. Rev. D45 (1992).

14. G. Altarelli, plenary talk at this Conference.

15. G. Passarino, Phys. Lett. 313B (1993) 213 and private communication.

16. G. Quast, talk at this Conference.

17. E. Braaten, S. Narison and A. Pich, Nucl. Phys. B373 (1992) 581; F. Le Diberder and A. Pich, Phys. Lett. 289B (1992) 165.

18. E. Fernández, plenary talk at this Conference.

19. ALEPH Coll., D. Buskulic et al., Phys. Lett. 307B (1993) 209.

20. J. Chyla and A.L. Kataev, Phys. Lett. 297B (1992) 385.

21. CCFR Coll., W.C. Leung et al., preprint NEVIS-1460 (1992).

22. See, for instance: R.K. Ellis, D.A. Ross and A.E. Terrano, Nucl. Phys. B178 (1981) 421; F. Aversa, P. Chiappetta, M. Greco and J.Ph. Guillet, Nucl. Phys. B327 (1989) 105; M. Mangano, P. Nason and G. Ridolfi, Nucl. Phys. B373 (1992) 295; Z. Kunszt and D.E. Soper, Phys. Rev. D 46 (1992) 196; W.T. Giele, E.W.N. Glower and D.A. Kosower, Nucl. Phys. B403 (1993) 633.

23. See, for instance: A. Bassetto, M. Ciafaloni and G. Marchesini, Phys. Rep. 100 (1983) 202; Yu.L. Dokshitzer, V.A. Khoze, A.H. Mueller and S.I. Troyan, *Basics of Perturbative QCD*, Editions Frontieres, Paris, 1991; and references therein.

24. Z. Bern and D.A. Kosower, Nucl. Phys. B379 (1992) 451.

25. R.K. Ellis and J.C. Sexton, Nucl. Phys. B269 (1986) 445.

26. Z. Bern, L. Dixon and D.A. Kosower, Phys. Rev. Lett. 70 (1993) 2677.

27. Z. Bern and D.C. Dunbar, Nucl. Phys. B379 (1992) 562; M.J. Strassler, Nucl. Phys. B385 (1992) 145.

28. *New Techniques for Calculating Higher Order QCD Corrections*, Proc. ETH Workshop, Zürich 1992, ed. Z. Kunszt, preprint ETH-TH/93-01.

29. Z. Kunszt, P. Nason, G. Marchesini and B.R. Webber, in 'Z Physics at LEP 1', CERN 89-08, vol. 1, p. 373.

30. S. Banerjee, talk at this Conference.

31. S. Bethke, preprint HD-PY 93/7.

32. L3 Coll., B. Adeva et al., Phys. Lett. 248B (1990) 464, Phys. Lett. 257B (1991) 469; ALEPH Coll., D. Decamp et al., Phys. Lett. 255B (1991) 623; DELPHI Coll., P. Abreu et al., Zeit. Phys. C54 (1992) 55; OPAL Coll., P.D. Acton et al., Zeit. Phys. C55 (1992) 1; S. Bethke and J.E. Pilcher, Ann. Rev. Nucl. Part. Sci. 42 (1992) 251.

33. S. Catani, G. Turnock, B.R. Webber and L. Trentadue, Phys. Lett. 263B (1991) 491.

34. S. Catani, G. Turnock and B.R. Webber, Phys. Lett. 272B (1991) 368, Phys. Lett. 295B (1992) 269.

35. J. Kodaira and L. Trentadue, Phys. Lett. 123B (1982) 335; J.C. Collins and D.E. Soper, Nucl. Phys. B197 (1982) 446, Nucl. Phys. B284 (1987) 253; G. Turnock, preprint Cavendish-HEP-92/3; R. Fiore, A. Quartarolo and L. Trentadue, Phys. Lett. 294B (1992) 431.

36. S. Catani, Yu.L. Dokshitzer, M. Olsson, G. Turnock and B.R. Webber, Phys. Lett. 269B (1991) 432.

37. S. Catani, Yu.L. Dokshitzer, F. Fiorani and B.R. Webber, Nucl. Phys. B377 (1992) 445, Nucl. Phys. B383 (1992) 419.

38. S. Catani, G. Turnock, B.R. Webber and L. Trentadue, Nucl. Phys. B407 (1993) 3.

39. ALEPH Coll., D. Decamp et al., Phys. Lett. 284B (1992) 163; L3 Coll., O. Adriani et al., Phys. Lett. 284B (1992) 471; OPAL Coll., P.D. Acton et al., preprint CERN-PPE/93-38; DELPHI Coll., P. Abreu et al., preprint CERN-PPE/93-43.

40. L3 Coll., S. Banerjee and S. Müller, L3 note 1441, presented at this Conference; OPAL Coll., internal note OPAL-PN102, presented at this Conference; SLD Coll., K. Abe et al., preprint SLAC-PUB-6133, submitted to this Conference; TOPAZ Coll., Y. Ohnishi et al., Phys. Lett. 313B (1993) 475.

41. JADE Coll., W. Bartel et al., Zeit. Phys. C33 (1986) 23.

42. S. Catani, in *QCD at 200 TeV*, Proc. 17th Eloisatron Project Workshop, eds. L. Cifarelli and Yu.L. Dokshitzer (Plenum Press, New York, 1992), pag. 21; Yu.L. Dokshitzer and M. Olsson, Nucl. Phys. B396 (1993) 137.

43. S. Bethke, Z. Kunszt, D.E. Soper and W.J. Stirling, Nucl. Phys. B370 (1992) 310; N. Brown and W.J. Stirling, Zeit. Phys. C53 (1992) 629.

44. T. Hebbeker, Phys. Rep. 217 (1992) 69.

45. N. Brown and W.J. Stirling, Phys. Lett. 252B (1990) 657.

46. S. Bethke, in Proc. of the Aachen Conf. *QCD - 20 Years Later*, eds. P.M. Zerwas and H.A. Kastrup (World Scientific, Singapore, 1993), pag. 43 and in Ref. [30]; B.R. Webber, in Proc. of the Aachen Conf. *QCD - 20 Years Later*, eds. P.M. Zerwas and H.A. Kastrup (World Scientific, Singapore, 1993), pag. 73.

47. S. Bethke, in Proc. of the 26th Int. Conf. on High Energy Physics, Dallas, August 1992, ed. J.R. Sanford (AIP, New York, 1993), pag. 81.

48. M. Gluck, E. Reya and A. Vogt, Zeit. Phys. C53 (1992) 127, Phys. Lett. 306B (1993) 391; A.D. Martin, W.J. Stirling and R.G. Roberts, Phys. Rev. D 47 (1993) 867, Phys. Lett. 306B (1993) 145; CTEQ Coll., J. Botts et al., Phys. Lett. 304B (1993) 159.

49. NMC, P. Amaudruz et al., Phys. Lett. 295B (1992) 159; NMC, M. Arneodo et al., Phys. Lett. 309B (1993) 222.

50. CCFR Coll., S.R. Mishra et al., preprint NEVIS-1459 (1992); CCFR Coll., P.Z. Quintas et al., Phys. Rev. Lett. 71 (1993) 1307.

51. J. Huth et al., in Proc. of *Research Directions for the Decade, Snowmass 1990*, ed. E.L. Berger (World Scientific, Singapore, 1992), pag. 134.

52. CDF Coll., F. Abe et al., Phys. Rev. D 45 (1992) 1448, Phys. Rev. Lett. 68 (1992) 1104.

53. D0 Coll., R.V. Astur, FERMILAB-CONF-93-047-E; D0 Coll., G.C. Blazey, FERMILAB-CONF-93-050-E.

54. S.D. Ellis, Z. Kunszt and D.E. Soper, Phys. Rev. D 40 (1989) 2188, Phys. Rev. Lett. 64 (1990) 2121, Phys. Rev. Lett. 69 (1992) 1496.

55. F. Aversa, P. Chiappetta, L. Gonzales, M. Greco and J.Ph. Guillet, Zeit. Phys. C49 (1991) 459.

56. S. Hahn, talk at this Conference; J.F. Glicenstein, talk at this Conference.

57. S.D. Ellis, Z. Kunszt and D.E. Soper, Phys. Rev. Lett. 69 (1992) 3615.

58. CDF Coll., F. Abe et al., Phys. Rev. Lett. 70 (1993) 1376.

59. S.D. Ellis, preprint CERN-TH.6861/93.

60. UA1 Coll., C. Albajar et al., Nucl. Phys. B309 (1988) 405; G. Marchesini and B.R. Webber, Phys. Rev. D 38 (1988) 3419.

61. OPAL Coll., internal note OPAL-PN105, presented at this Conference.

62. CDF Coll., F. Abe et al., Phys. Rev. Lett. 70 (1993) 713.

63. S. Catani, Yu.L. Dokshitzer and B.R. Webber, Phys. Lett. 285B (1992) 291.

64. S. Catani, Yu.L. Dokshitzer, M.H. Seymour and B.R. Webber, Nucl. Phys. B406 (1993) 187.

65. S.D. Ellis and D.E. Soper, CERN preprint CERN-TH.6860/93.

66. M.H. Seymour, preprint LU-TP-93-8.

67. A. Rostovtsev, talk at this Conference.

68. I.H. Park, talk at this Conference.

69. E. Witten, Nucl. Phys. B120 (1977) 189; C.H. Llewellyn Smith, Phys. Lett. 79B (1978) 83.

70. H1 Coll., T. Ahmed et al., Phys. Lett. 297B (1992) 205; ZEUS Coll., M. Derrick et al., Phys. Lett. 297B (1992) 404.

71. See *Physics at HERA*, Proc. of the 1991 DESY Workshop, eds. W. Buchmüller and G. Ingelman (DESY, Hamburg, 1992), vol. 3.

72. L.E. Gordon and J.K. Storrow, Phys. Lett. 291B (1992) 320; G. Kramer and S.G. Salesch, preprint DESY 93-010; M. Greco and A. Vicini, preprint LNF-93/017-P.

73. D. Bödeker, preprint DESY 92-188.

74. H1 Coll., T. Ahmed et al., Phys. Lett. 298B (1993) 469; ZEUS Coll., M. Derrick et al., Phys. Lett. 306B (1993) 158, Zeit. Phys. C59 (1993) 231.

75. E665 Coll., M.R. Adams et al., Phys. Rev. Lett. 69 (1992) 1026.

76. H1 Coll., I. Abt et al., preprint DESY 93-137.

77. J.G. Körner, E. Mirkes and G.A. Schuler, Int. J. Mod. Phys. A4 (1989) 1781; D. Graudenz and M. Magnussen, in *Physics at HERA*, Proc. of the 1991 DESY Workshop, eds. W. Buchmüller and G. Ingelman (DESY, Hamburg, 1992), pag. 261.

78. T. Brodkorb and J.G. Körner, Zeit. Phys. C54 (1992) 519; D. Graudenz, preprint LBL-34147 (1993).

79. L. Lönnblad, Zeit. Phys. C58 (1993) 471; B.R. Webber, preprint CERN-TH.6871/93.

80. A.X. El-Khadra, G. Hockney, A.S. Kronfeld and P.B. Mackenzie, Phys. Rev. Lett. 69 (1992) 729.

81. G. Altarelli, in Proc. of the Aachen Conf. *QCD - 20 Years Later*, eds. P.M. Zerwas and H.A. Kastrup (World Scientific, Singapore, 1993), pag. 172.

82. C.T. Sachrajda, plenary talk at this Conference.

83. S. Bethke and S. Catani, in *Perturbative QCD and Hadronic Interactions*, Proc. 27th Recontres de Moriond, ed. J. Tran Thanh Van (Editions Frontieres, Gif-sur-Yvette, 1992), pag. 203; I. Hinchliffe, preprint LBL-33952, to appear in *Electroweak Interactions and Unified Theories*, Proc. 28th Recontres de Moriond, Les Arcs, March 1993.

84. P. Aurenche, R. Baier, A. Douiri, M. Fontannaz and D. Schiff, Phys. Lett. 140B (1984) 87; H. Baer, J. Ohnemus and J.F. Owens, Phys. Rev. D42 (1990) 61; P. Aurenche, P. Chiappetta, M. Fontannaz, J.Ph. Giullet and E. Pilon, Nucl. Phys. B399 (1993) 34.

85. P. Nason, S. Dawson and R.K. Ellis, Nucl. Phys. B303 (1988) 607; W. Beenakker, W.L. van Neerven, R. Meng, G.A. Schuler and J. Smith, Nucl. Phys. B351 (1991) 507; E.L. Berger, R. Meng and W.K. Tung, Phys. Rev. D 46 (1992) 1895; E.L. Berger, R. Meng and J. Qiu, in Proc. of the 26th Int. Conf. on High Energy Physics, Dallas, August 1992, ed. J.R. Sanford (AIP, New York, 1993), pag. 853.

86. B. Barnett, talk at this Conference.